

Hybrid improved EMD-BPNN model for the prediction of sea surface temperature

Zhiyuan Wu^{a,b,c}, Changbo Jiang^{a,c,*}, Mack Conde^d, Bin Deng^{a,c}, Jie Chen^{a,c}

a. School of Hydraulic Engineering, Changsha University of Science & Technology, Changsha, 410004, China;

b. School for Marine Science and Technology, University of Massachusetts Dartmouth, New Bedford, MA 02744, USA;

c. Key Laboratory of Water-Sediment Sciences and Water Disaster Prevention of Hunan Province, Changsha, 410004, China;

d. Department of Mathematics, University of Massachusetts Dartmouth, North Dartmouth, MA 02747, USA.

Highlights

- A SST predicting method based on the hybrid EMD algorithms and BP neural network method is proposed in this paper.
- SST prediction results based on the hybrid EEMD-BPNN and CEEMD-BPNN models are compared and discussed.
- Cases study of SST in the North Pacific shows that the proposed hybrid CEEMD-BPNN model can effectively predict the time-series SST.

Abstract: Sea surface temperature (SST) is the major factor that affects the ocean-atmosphere interaction, and in turn the accurate prediction of SST is the key to ocean dynamic prediction. In this paper, an SST predicting method based on empirical mode decomposition (EMD) algorithms and back-propagation neural network (BPNN) is proposed. Two different EMD algorithms have been applied extensively for analyzing time-series SST data and some nonlinear stochastic signals. Ensemble empirical mode decomposition (EEMD) algorithm and Complementary Ensemble Empirical Mode Decomposition (CEEMD) algorithm are two improved algorithms of EMD, which can effectively handle the mode-mixing problem and decompose the original data into more stationary signals with different frequencies. Each Intrinsic Mode Function (IMF) has been taken as input data to the back-propagation neural network model. The final predicted SST data is obtained by aggregating the predicted data of individual IMF. A case study, of the monthly mean SST anomaly (SSTA) in the northeastern region of the North Pacific, shows that the proposed hybrid CEEMD-BPNN model is much more accurate than the hybrid EEMD-BPNN model, and the prediction accuracy based on BP neural network is improved by the CEEMD method. Statistical analysis of the case study demonstrates that applying the proposed hybrid CEEMD-BPNN model is effective for the SST prediction.

30

31 **Keywords.**

32 Sea Surface Temperature; Back-Propagation Neural Network; Empirical Mode Decomposition; Prediction;
33 Machine Learning Algorithms.

34

35 **1 Introduction**

36 The Sea Surface Temperature (SST) is a main factor in the interaction between the ocean and the
37 atmosphere (Wiedermann et al., 2017; He et al., 2017; Wu et al., 2019a), and it characterizes the combined
38 results of ocean heat (Buckley et al., 2014; Griffies et al., 2015; Wu et al., 2019b), dynamic processes
39 (Takakura et al., 2018). It is a very important parameter for climate change and ocean dynamics process,
40 reflects sea-air heat and water vapor exchange. Small changes in sea temperature can have a huge impact on
41 the global climate. The well-known El Niño and La Niña phenomena are caused by abnormal changes in SST
42 (Chen et al., 2016a; Zheng et al., 2016).

43 Therefore, scholars have begun to observe the SST in recent years, the observation of the SST is
44 important (Kumar et al., 2017; Sukresno et al., 2018). Accurate observation and effective prediction of the
45 SST are very important (Hudson et al., 2010). Predicting the SST in advance can enable people to take
46 appropriate measures to reduce the impact on daily life and reduce unnecessary losses. However, due to the
47 high randomness and irregular of the monthly mean sea surface temperature anomaly (SSTA), the nonlinear
48 and non-stationary characteristics are obvious. At present, there is no clear and feasible method with high
49 accuracy to effectively predict the SST (Zhu et al., 2015; Chen et al., 2016b; Khan et al., 2017).

50 In mathematics and science, a nonlinear system is a system in which the change of the output is not
51 proportional to the change of the input. Nonlinear dynamical systems, describing changes in variables over
52 time, may appear chaotic, unpredictable, or counterintuitive, contrasting with much simpler linear systems.
53 A stationary process is a stochastic process whose unconditional joint probability distribution does not change
54 when shifted in time. Consequently, statistical parameters such as mean and variance also do not change over
55 time. The variation of SST is a deterministic non-linear dynamic system and a non-stationary time series data.
56 Empirical Mode Decomposition (EMD) is a state-of-the-art signal processing method proposed by Huang et
57 al. (1998). This method can decompose the signal data of different frequencies step by step according to the
58 characteristics of the data and obtain several orthogonal components and a trending component (Wang et al.,
59 2015; Amezquita-Sanchez and Adeli,2015; Wang et al., 2016; Kim and Cho, 2016). The empirical mode

60 decomposition (EMD) method is powerful and adaptive in analyzing nonlinear and non-stationary data sets.
61 It provides an effective approach for decomposing a signal into a collection of so-called intrinsic mode
62 functions (IMFs), which can be treated as empirical basis functions (Duan et al., 2016). However, there were
63 some problems with the EMD method, such as mode mixing (Huang and Wu, 2008; Wu et al., 2008; Wu and
64 Huang, 2009).

65 Once an intermittent signal appears in the actual signal, the EMD decomposition method will produce
66 a Mode Mixing Problem. The Mode Mixing Problem causes the essential modal function (IMFs) to lose its
67 physical meaning. This is defined as either a single IMF consisting of widely disparate scales, or a signal of
68 similar scale captured in different IMF's. To overcome mode mixing two noise assisted methods have
69 emerged. Ensemble Empirical Mode Decomposition (EEMD) adds a fixed percentage of white noise to the
70 signal before decomposing it. This step is repeated N times after which all results are averaged. EEMD
71 improves the mode-mixing problem but it cannot completely reconstruct the input signal from the resulting
72 components. Complete Ensemble Mode Decomposition (CEEMD) is also a noise-assisted method. Similarly
73 the method decomposes the signal with N different noise realizations but here the results are averaged after
74 each component is found. CEEMD solves the mode mixing problem and it provides an exact reconstruction
75 of the input signal.

76 Wu and Huang (2009) proposed the Ensemble Empirical Mode Decomposition (EEMD) method by
77 adding different white noise in each ensemble member to suppress mode mixing. Yeh et al. (2010) added two
78 opposite-signal white noises to the time-series data sequence, and proposed an improved algorithm for
79 EEMD, Complete Ensemble Empirical Mode Decomposition (CEEMD). The decomposition effect is
80 equivalent to EEMD, and the reconstruction error caused by adding white noise is reduced (Tang et al., 2015).
81 At present, the EMD model and its improved algorithms had been widely used in many fields on ocean
82 science, such as storm surge and sea level rise (Wu et al., 2011; Lee, 2013; Ezer and Atkinson, 2014), tidal
83 amplitude (Cheng et al., 2017; Pan et al., 2018) and wave height (Duan et al., 2016; Sadeghifar et al., 2017;
84 López et al., 2017). These studies and applications reflected that the EMD model and its improved algorithms
85 can effectively reduce the non-stationarity of the time-series data, which helps further analysis and processing.

86 The ensemble empirical mode decomposition (EEMD) method is a noise assisted empirical mode
87 decomposition algorithm. The CEEMD works by adding a certain amplitude of white noise to a time series,
88 decomposing it via EMD, and saving the result. In contrast to the EEMD method, the CEEMD also ensures
89 that the IMF set is quasi-complete and orthogonal. The CEEMD can ameliorate mode mixing and

90 intermittency problems. The CEEMD is a computationally expensive algorithm and may take significant
91 time to run.

92 For nonlinear prediction, the more commonly used methods are curve fitting (Motulsky and Ransnas,
93 1987), gray-box model (Pearson and Pottmann, 2000), homogenization function model (Monteiro et al.,
94 2008), neural network (Deo et al., 2001; Wang et al, 2015; Kim et al., 2016) and so on. Among them, Back-
95 Propagation Neural Network (BPNN) (Lee, 2004; Jain and Deo, 2006; Savitha and Al, 2017; Wang et al.,
96 2018) has certain advantages in dealing with nonlinear problems, it is a basic machine learning algorithm
97 and its principle is simple and operability is strong, so in ocean science and engineering it has been widely
98 used.

99 In view of non-stationary and nonlinear monthly mean SST, the EEMD, CEEMD and BP neural network
100 will be used here to study how to improve the accuracy of SST prediction. The hybrid EMD-BPNN models
101 will be established for the prediction of SSTA in the northeastern region of the Pacific Ocean.

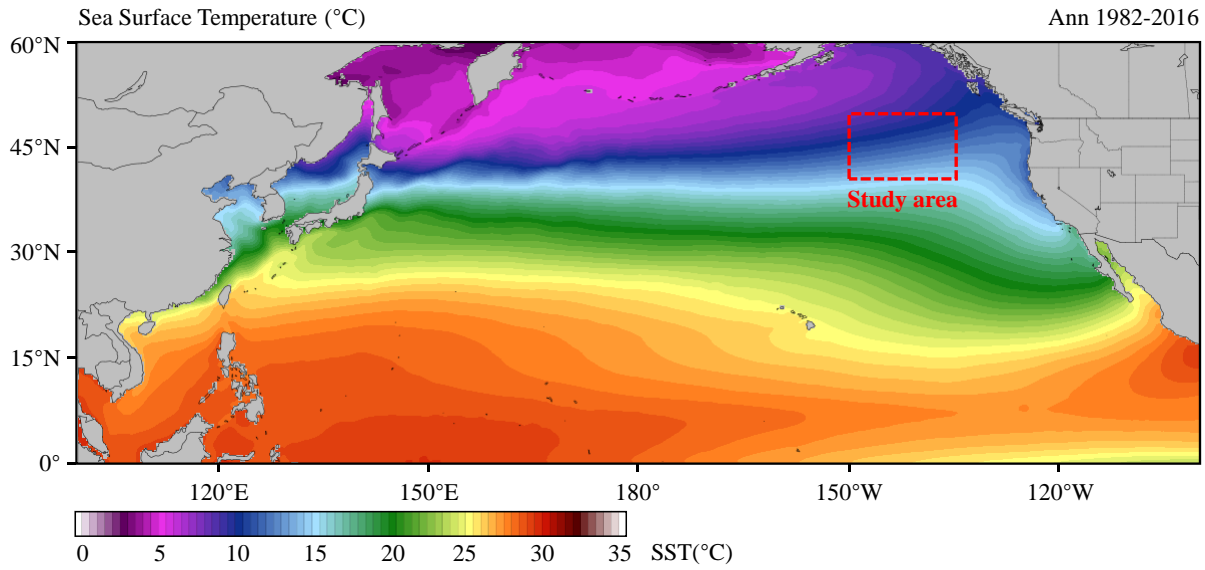
102 **2 Data collection**

103 The SST time-series data in this study is from the NOAA Optimum Interpolation Sea Surface
104 Temperature (OISST) official website (Reynolds et al., 2007; Banzon et al., 2016;
105 <https://www.ncdc.noaa.gov/oisst/data-access>). The NOAA 1/4°daily OISST is an analysis constructed by
106 combining observations from different platforms (satellites, ships, buoys) on a regular global grid. There are
107 two kinds of OISST, named after the relevant satellite SST sensors. These are the Advanced Very High
108 Resolution Radiometer (AVHRR) and Advanced Microwave Scanning Radiometer on the Earth Observing
109 System (AMSR-E); the AVHRR dataset is used in this study. The average annual sea surface temperature in
110 North Pacific (0°N-60°N, 100°E-100°W) from January 1982 to December 2016 is shown in Fig.1.

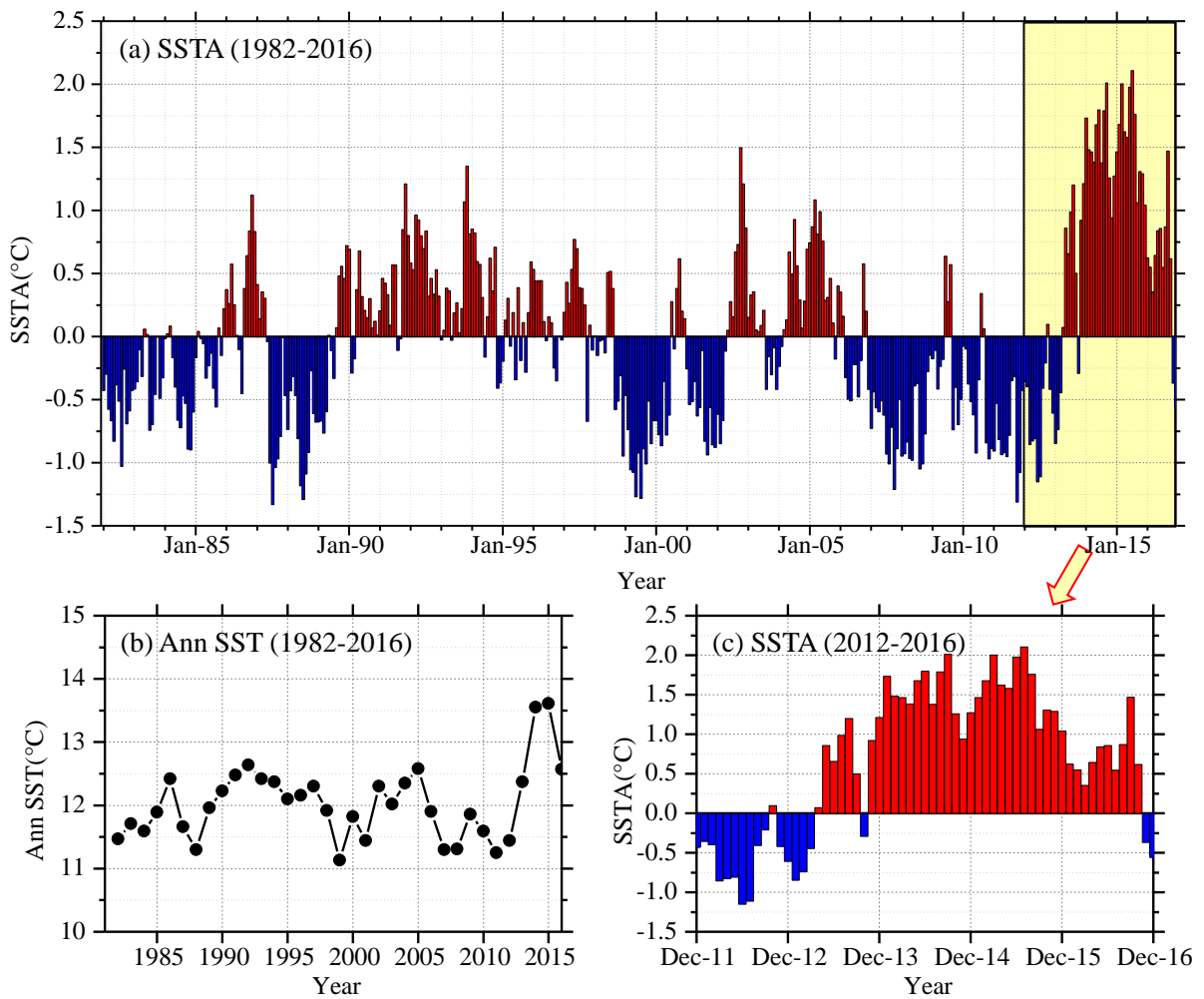
111 It has been shown that the sea surface temperature anomaly in the northeastern Pacific in the ten years
112 2006-2016 was 2.0°C warmer than in the previous ten years 1996-2006. Previous studies (Bond et al., 2015)
113 showed that in the spring and summer of 2014, the high SST area of the northeastern Pacific had expanded
114 to coastal ocean waters, which affected the weather in coastal areas and the lives of fishermen, and even
115 affected the temperature in Washington, USA, causing interference to daily life.

116 In this study, we select the northeastern region of the North Pacific Ocean (in Fig.1, 40°N-50°N, 150°W-
117 135°W) to measure sea surface temperature. The time-series data of SST for the study area from January
118 1982 to December 2016 with a data length of 420 months was obtained from OISST-V2 (Fig. 2). The monthly
119 mean sea surface temperature anomaly (SSTA) was used in the analysis and calculation. As shown in Fig.

120 2(a), it can be found the overall time-series data is very messy, nonlinear and random from the perspective
 121 of the image.



122
 123 **Fig.1** Average annual sea surface temperature in North Pacific during Jan 1982 to Dec 2016 (35-years).



124
 125 **Fig.2** The time-series of sea surface temperature in the study area. (a) SST anomaly (1982-2016, 35 years);

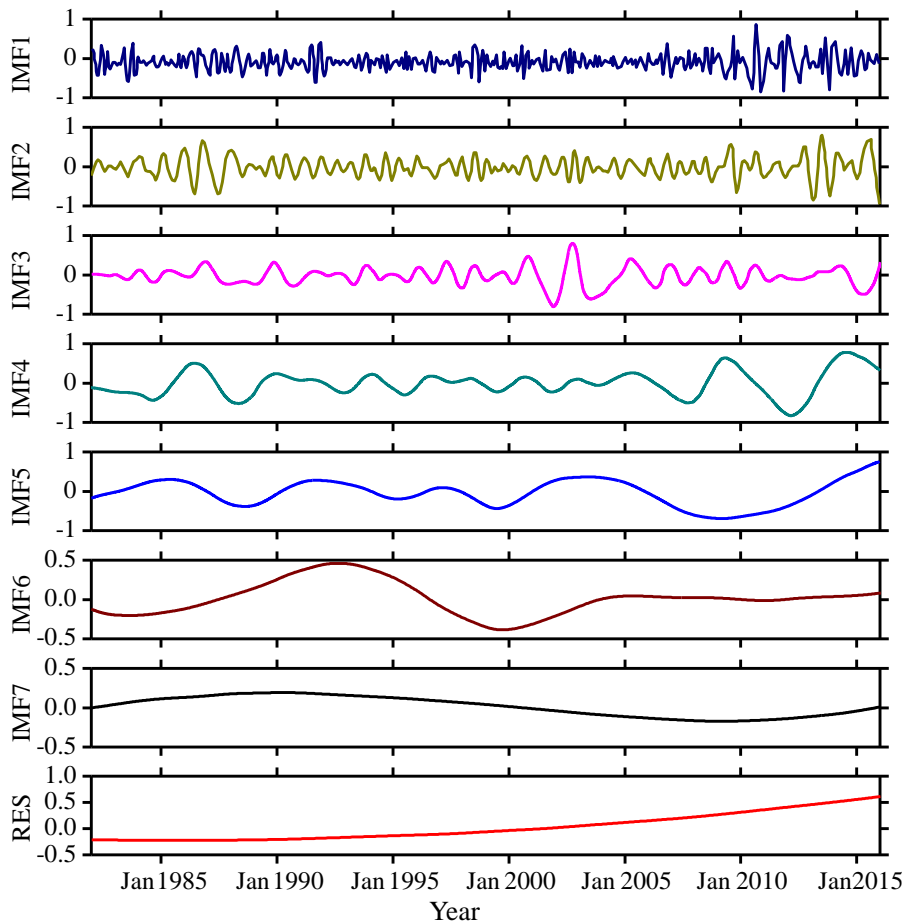
126 (b) Annual SST (1982-2016, 35 years); (c) SST anomaly (2012-2016, 5 years).

127 **3 Decomposition of SSTA**

128 The purpose of this study is to combine the EEMD algorithm and the CEEMD decomposition algorithm
129 respectively with the BP neural network algorithm to establish a prediction model, a hybrid EMD-BPNN
130 model. The EEMD and CEEMD algorithms are performed on the monthly mean SSTA data to obtain a series
131 of intrinsic mode functions (IMFi). Each IMFi is predicted by a BP neural network and then the IMFi are
132 recombined to obtain the predicted value of SSTA.

133 **3.1 Decomposition by the EEMD algorithm**

134 The SSTA in Fig. 2(a) has been decomposed based on the ensemble empirical mode decomposition
135 (EEMD algorithm), and seven IMF components and a residual component RES (Residue) are obtained as
136 shown in Fig. 3.



137
138 **Fig.3** IMF components and the trend item RES of monthly mean SSTA over the study area based on the
139 EEMD algorithm during 1982-2016.

140

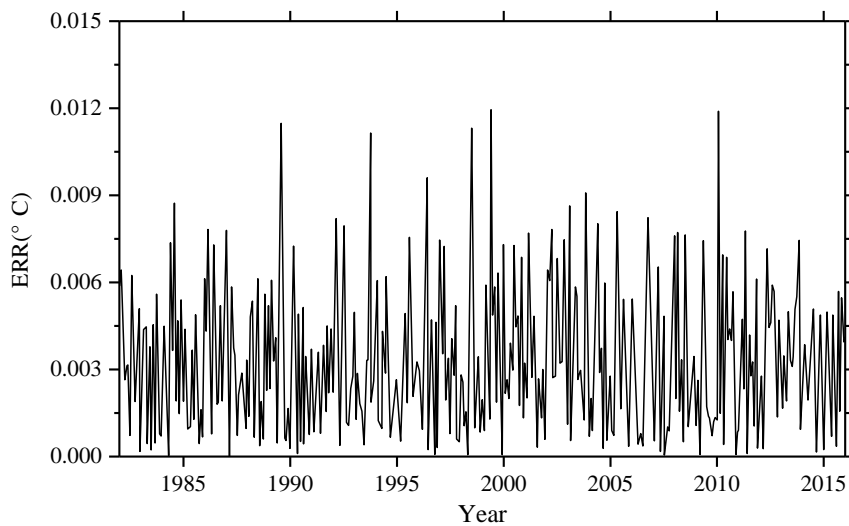
141 It can be seen from Fig. 3 that the first three intrinsic mode function components IMF1, IMF2, and IMF3
 142 still exhibit strong non-stationarity because they have strong irregular oscillations and periodic changes. The
 143 IMF4 to IMF7 and the final trend term RES have some periodicity and relatively regular fluctuation, and the
 144 non-stationary properties are less than the first three components. The trend term RES reflects that the overall
 145 trend of SSTA has gradually increased since 1982. As the non-stationarity of IMF i decreases with increasing
 146 i , the EEMD algorithm will reduce the influence of non-stationarity on prediction. The absolute error (ERR)
 147 of the decomposition can be calculated by the following Formula (1).

$$148 \quad a(t) = \left| S(t) - \left[\sum_{i=1}^7 I_i(t) + R(t) \right] \right| \quad (1)$$

149 where, $a(t)$ is the absolute error (ERR), $S(t)$ the original SSTA observation data, $I_i(t)$ the i -th component
 150 of the IMF (IMF i), and $R(t)$ the trend term (RES).

151 The absolute error (ERR) based on the EEMD algorithm is shown in Fig. 4. It can be seen from the
 152 figure that the ERR of 420 months after decomposition is basically below 0.01 °C, and the ERR exceeds
 153 0.01 °C in five months: June 1989, September 1993, July 1998, May 1999 and March 2010.

154 In addition to June 1989, the other four monthly data with a large ERR occurred during the El Niño
 155 period. The maximum error is in March 2010, the actual value is -0.1204 °C, the result based on EEMD
 156 algorithm is -0.1325 °C, the ERR of decomposition is 0.0121 °C; the minimum error, in April 1987, is
 157 1.73×10^{-5} °C. The overall mean ERR based on the EEMD algorithm is 0.0035 °C.

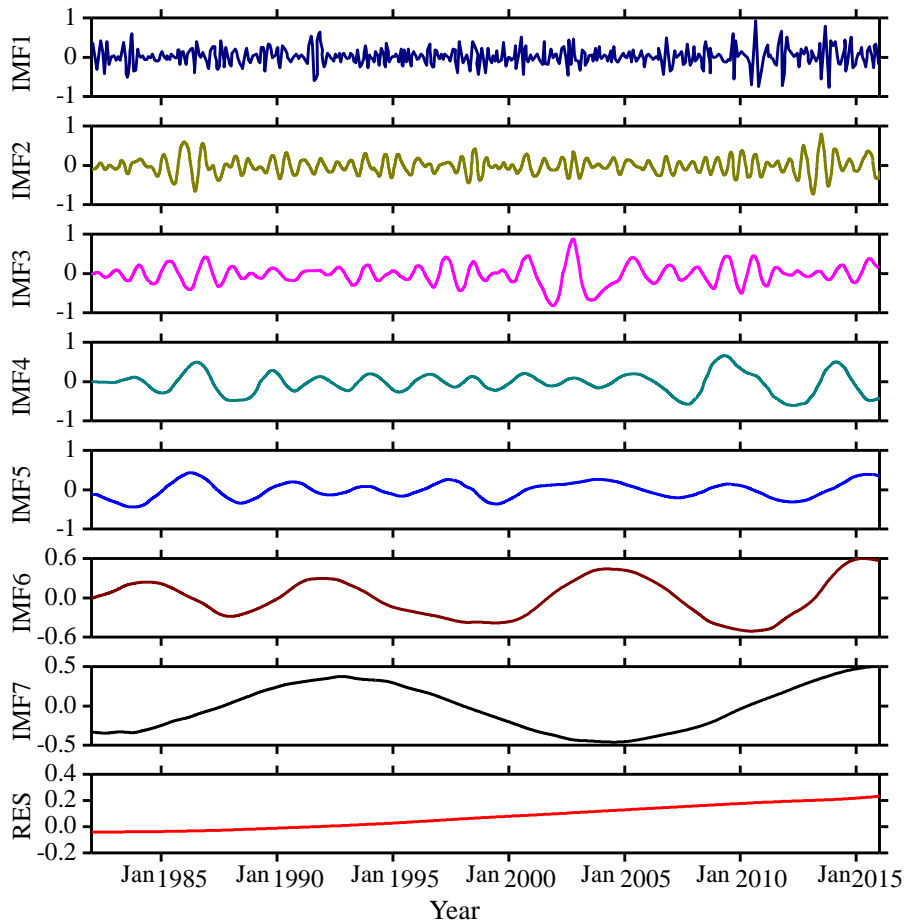


158
 159 **Fig. 4** The ERR of monthly mean SSTA over the study area based on the EEMD algorithm during 1982-2016.

160

161 **3.2 Decomposition by the CEEMD algorithm**

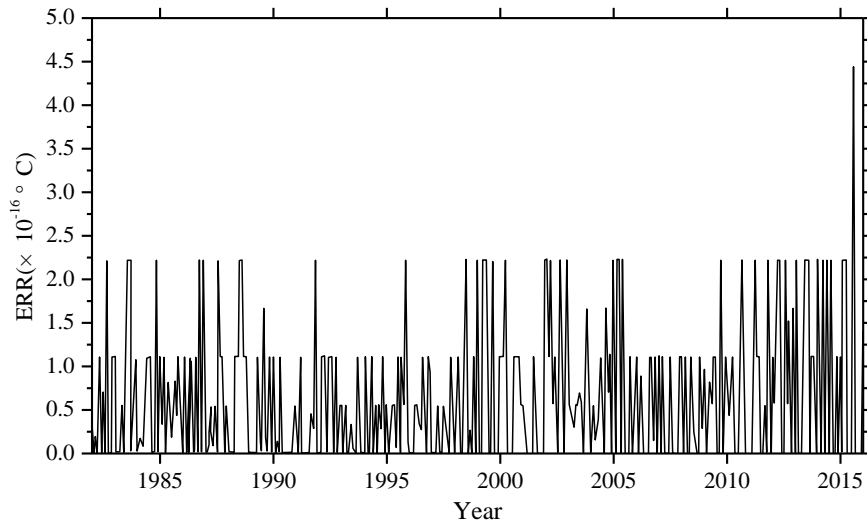
162 The SSTA has been decomposed based on the complementary ensemble empirical mode decomposition
163 (CEEMD algorithm) and seven IMF components and a residual component RES (Residue) are obtained as
164 shown in Fig. 5. It can be seen when comparing the decomposition results based on EEMD and CEEMD
165 algorithms that although the mode components decomposed by CEEMD algorithm are different from the
166 corresponding results decomposed by EEMD, the non-stationarities of the seven modes decomposed by the
167 two decomposition algorithms are gradually decreasing, and the final trend term RES is an upward trend.
168 Both decomposition algorithms confirm the characteristic of a gradual increase in the overall trend of the
169 data series.



170
171 **Fig.5** IMF components and the trend item RES of monthly mean SSTA over the study area based on the
172 CEEMD algorithm during 1982-2016.

173
174 The absolute error (ERR) obtained based on the CEEMD algorithm is shown in Fig. 6. It can be seen
175 from the figure that the ERR of 420 months data after decomposition is less than $5 \times 10^{-16} \text{ }^\circ\text{C}$, and the accuracy

176 is very better. The maximum error is $4.48 \times 10^{-16} \text{ }^\circ\text{C}$ in March 2016; the minimum error is zero. The overall
177 mean ERR based on CEEMD algorithm is $6.10 \times 10^{-17} \text{ }^\circ\text{C}$. By comparing the results and errors of the above
178 two decomposition algorithms, it can be seen that the error based on the improved algorithm (CEEMD) is
179 much smaller than the error based on the EEMD algorithm. Because more white noise with the opposite
180 sign had been added in CEEMD algorithm, the reconstruction error caused by the white noise has been
181 reduced over it in EEMD algorithm.



182
183 **Fig. 6** The ERR of monthly mean SSTA over the study area based on the CEEMD algorithm during 1982-
184 2016.

185
186 **4 SSTA prediction model**

187 **4.1 The BP neural network**

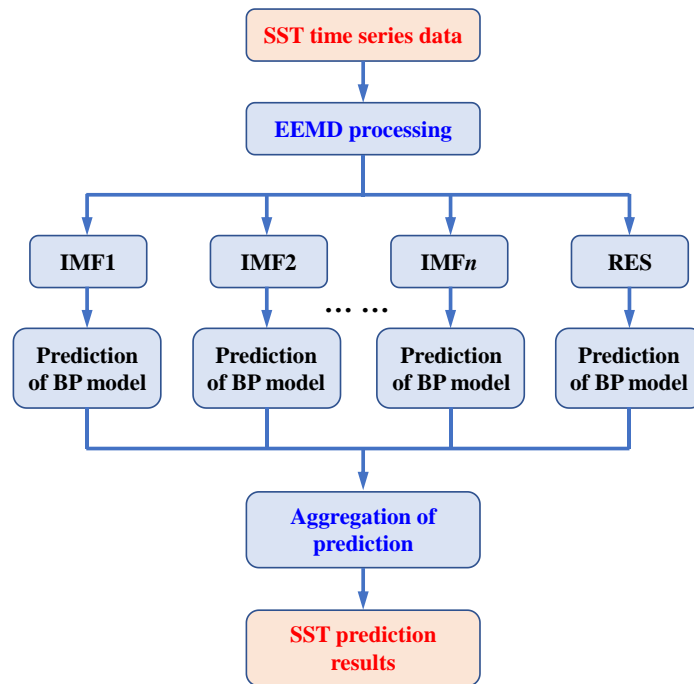
188 Artificial Neural Network (ANN) is an information processing approach based on the biological neural
189 network (López et al., 2015; Kim et al., 2016). In theory, ANN can simulate any complex nonlinear
190 relationship through nonlinear units (neurons) and has been widely used in the prediction area, such as wave
191 height and storm surge. The most basic structure of ANN consists of input layers, hidden layers and output
192 layers. One of the most widely used ANN models is the back propagation neural network (BPNN, Wang et
193 al., 2018) algorithm based on the BP algorithm.

194 The BPNN algorithm is a multi-layer feedforward network trained according to the error back
195 propagation algorithm and is one of the most widely used deep learning algorithms. The BP network can be
196 used to learn and store a large number of mappings of input and output models without the need to publicly

197 describe the mathematical equations of these mapping relationships. The learning rule is to use the steepest
 198 descent method. When applied to SST predicting, the input data are monthly mean SST in previous months
 199 and the output data are predicted SST time-series data. The desired data for comparison is the observed actual
 200 SST.

201 **4.2 SSTA prediction model based on hybrid improved EMD-BPNN algorithm**

202 The proposed monthly mean sea surface temperature anomaly (SSTA) predicting model includes three
 203 steps as follows. First, original SST datasets are decomposed into certain more stationary signals with
 204 different frequencies by EEMD. Second, the BP neural network is used to predict each IMF and the residue
 205 RES. A rolling forecasting process is studied. The prediction is made using the previous data for one step
 206 ahead. Finally, the prediction results of each IMF and the residue RES are aggregated to obtain the final SST
 207 prediction results. The flowchart of the SST prediction model based on hybrid improved empirical mode
 208 decomposition algorithm (improved EMD algorithm) and back-propagation neural network (BPNN) is shown
 209 in Fig. 7. The SST prediction model has been abbreviated as a hybrid improved EMD-BPNN model in the
 210 following article.



211
 212 **Fig.7** The flowchart of SST prediction model based on hybrid improved empirical mode decomposition
 213 algorithm (improved EMD algorithm) and back-propagation neural network (BPNN).

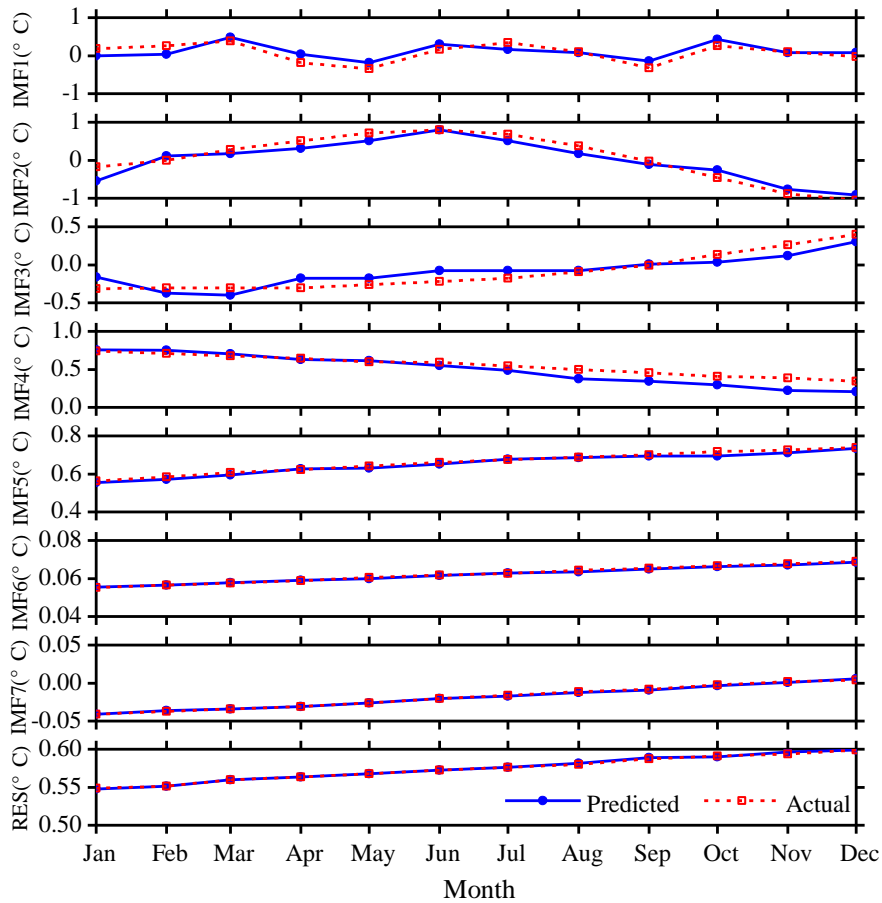
214

215 **5 Case study: SSTA prediction based on the hybrid improved EMD-BPNN models**

216 In order to study the effects of the two improved EMD algorithms (EEMD and CEEMD) on the
 217 prediction results, and to analyze the prediction ability of BP neural network, the following experiments were
 218 carried out. Predict SSTA results in 2017 and analyze the prediction abilities of different mode decomposition
 219 data based on EEMD and CEEMD algorithms. The experiment content is as follows: the BP neural network
 220 is trained with the decomposition data of each mode from 1982 to 2016, and the SSTA in 2017 is predicted
 221 by the trained neural network, and the observation results of 12 months in 2017 are used to compare and
 222 analyze with the prediction results.

223 A three-layer BP neural network structure has been chosen and independently analyze and predict each
 224 month. For the IMF4 and subsequent modes, the non-stationarity have been degraded relative to the first
 225 three modes, a BP neural network with 12 nodes at input layer and output layer has been used to train and
 226 predict SSTA.

227 The prediction results of each mode decomposition component based on the EEMD algorithm are shown
 228 in Fig. 8. The absolute errors of the predicted value and the actual value are shown in Table 1.



229
 230 **Fig. 8** SSTA prediction results based on the hybrid EEMD-BPNN model of each individual component in
 231 2017.

232 Root mean square error (RMSE) is used as metrics to access the performance of the two different models.

$$233 \quad \text{RMSE} = \sqrt{\frac{1}{N} \sum_{n=1}^N (x_n - y_n)^2} \quad (2)$$

234 where, x_n and y_n are the observed and the predicted values respectively, N is the number of data used for
 235 the performance evaluation and N is 12 in this study. Results are shown in Table 1.

236

237 **Table 1.** The absolute errors ERRs of the SSTA prediction results of each individual component based on the
 238 hybrid EEMD-BPNN model (unit: °C).

	Max ERR	Min ERR	Mean ERR	RMSE
IMF1	0.2197	0.0014	0.1424	0.1486
IMF2	0.2166	0.0323	0.1297	0.1673
IMF3	0.1872	0.0051	0.1070	0.1245
IMF4	0.1602	1.6869×10^{-4}	0.0663	0.0857
IMF5	0.0158	0.0010	0.0089	0.0104
IMF6	3.8766×10^{-4}	1.9752×10^{-4}	2.7221×10^{-4}	0.0003
IMF7	5.2662×10^{-4}	1.6387×10^{-4}	1.7907×10^{-4}	0.0002
RES	5.4859×10^{-4}	2.2308×10^{-4}	2.7766×10^{-4}	0.0003

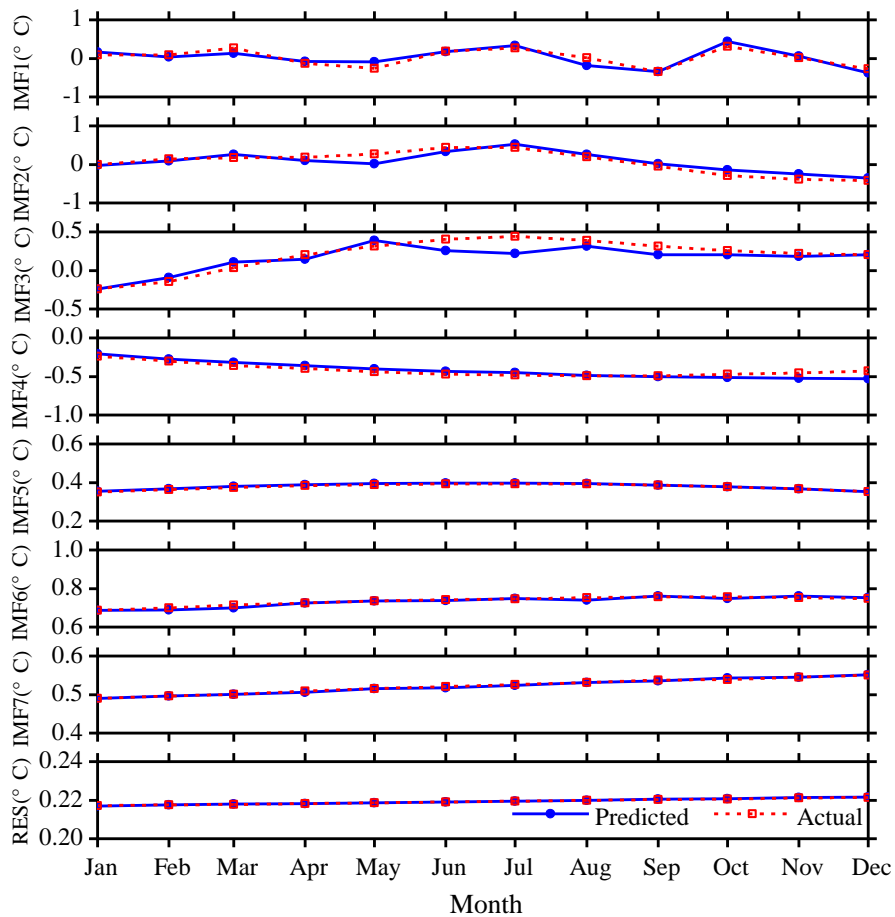
239

240 It can be seen from Fig. 8 and Table 1 that the maximum absolute error (Max ERR) of the first
 241 decomposition component IMF1 based on the hybrid EEMD-BPNN model is 0.2197 °C in January. The
 242 minimum absolute error (Min ERR) is 0.0014 °C, which is in August. The prediction ability of the second
 243 mode decomposition component IMF2 is roughly equivalent to the IMF1, and the mean absolute error (Mean
 244 ERR) of the first three intrinsic mode function components IMF1, IMF2, and IMF3 are between 0.10 °C and
 245 0.15 °C. The mean absolute errors of the IMF4 and IMF5 are 0.0663 °C and 0.0089 °C, respectively, and the
 246 prediction accuracy based on the hybrid EEMD-BPNN model is roughly equivalent to the decomposition
 247 accuracy of the EEMD algorithm. The prediction errors of the last two intrinsic mode function components
 248 and the residue RES are on the order of 10^{-4} . It can be seen that as the non-stationarity of the series data
 249 decreases, the error of the prediction results becomes smaller and smaller.

250 According to the same method, the eight mode components decomposed by CEEMD algorithm have
 251 been analyzed and predicted. The prediction results and error analysis have been shown in Fig. 9 and Table

252 2. It can be seen from Fig. 9 and Table 2 that the maximum error of the first decomposition component IMF1
 253 based on the hybrid CEEMD-BPNN model is 0.1779 °C in May. The minimum error is 0.0068 °C, which is
 254 in June.

255 The prediction ability of the second mode decomposition component IMF2 is roughly equivalent to the
 256 IMF1. Except for the four months of May, September, October, and November, the accuracies of prediction
 257 results of other months are satisfactory. The prediction results of the first three intrinsic mode function
 258 components IMF1, IMF2, and IMF3 are basically the same as the actual data. In the prediction results of the
 259 fourth mode component IMF4, except for a slight error in December, the prediction ability is better. The
 260 predicted results of the last three intrinsic mode function components IMF5, IMF6, IMF7 and the residue
 261 RES are basically consistent with the observation results.



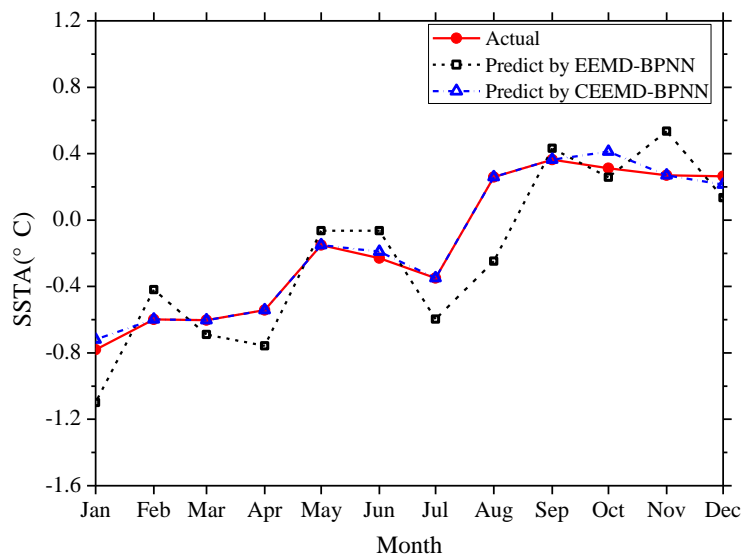
262
 263 **Fig. 9** SSTA prediction results based on the hybrid CEEMD-BPNN model of each individual component in
 264 2017.

265

266 **Table 2.** The absolute errors ERRs of the SSTA prediction results of each individual component based on the
 267 hybrid CEEMD-BPNN model (unit: °C).

	Max ERR	Min ERR	Mean ERR	RMSE
IMF1	0.1779	0.0068	0.0827	0.0987
IMF2	0.1643	0.0413	0.0811	0.1124
IMF3	0.1521	0.0160	0.0713	0.1006
IMF4	0.0851	0.0211	0.0324	0.0427
IMF5	0.0052	8.7694×10^{-5}	0.0021	0.0029
IMF6	0.0103	5.7748×10^{-5}	0.0043	0.0056
IMF7	0.0017	3.6026×10^{-5}	9.1374×10^{-4}	0.0010
RES	3.0342×10^{-5}	2.0163×10^{-6}	1.1572×10^{-5}	1.5017×10^{-5}

268
 269 The prediction results of the monthly mean SSTA in 2017 are obtained by reconstructing the mode
 270 decomposition components (Fig. 10) and the absolute error (ERR) of prediction results have been shown in
 271 Table 3. It can be seen from the figure and table that the prediction results based on the EEMD-BPNN model
 272 have larger ERRs in January and August, exceeding 0.3 °C, and the accuracies of prediction results in other
 273 months are satisfactory (the ERR is less than 0.3). The prediction accuracy based on the CEEMD-BPNN
 274 model is satisfactory, except for the ERR exceeding 0.1 °C in October, and the prediction ability based on
 275 the CEEMD-BPNN model is generally better than that of the EEMD-BPNN model.



276
 277 **Fig. 10** Monthly SSTA prediction results based on the hybrid improved EMD-BPNN models in 2017.

278 **Table 3.** The absolute errors ERRs of the SSTA prediction results based on the two different hybrid improved
 279 EMD-BPNN models (unit: °C).

	EEMD-BPNN model	CEEMD-BPNN model		EEMD-BPNN model	CEEMD-BPNN model
Jan	0.3188	0.0623	Sep	0.0687	0.0132
Feb	0.1780	0.0103	Oct	0.0545	0.1607
Mar	0.0867	0.0063	Nov	0.2651	0.0101
Apr	0.2153	0.0137	Dec	0.1290	0.0183
May	0.0854	0.0102	Min ERR	0.0545	0.0063
Jun	0.1662	0.0224	Max ERR	0.5068	0.1607
Jul	0.2474	0.0077	Mean ERR	0.1935	0.0289
Aug	0.5068	0.0112	RMSE	0.2299	0.0512

280

281 The correlation coefficient between the prediction values based on the CEEMD-BPNN model and
 282 observations is 0.97 indicating a significance level of 0.001. The result indicates that SSTA in 2017 was
 283 predicted accurately by the CEEMD-BPNN model. As can be seen from the above discussions, the ERR of
 284 decomposition components based on the EEMD and CEEMD algorithms will affect the accuracy of the final
 285 prediction results. Table 3 shows that prediction results of the hybrid CEEMD and BPNN model are much
 286 better than with the EEMD-BPNN. This is because after CEEMD, the original unsteady data are changed
 287 into certain components that have fixed frequency and periodicity. The CEEMD algorithm with less
 288 decomposition error has less error in the final prediction results, which proves that the CEEMD method has
 289 more advantages in data decomposition than the EEMD method. At the same time, we can find that the final
 290 prediction error of the two prediction models mainly comes from the first three mode decomposition
 291 components, and the error of the last five components has little effect on the accuracy of the final prediction
 292 results.

293

294 **6 Conclusions**

295 This paper presents an SST predicting method based on the hybrid EMD algorithms and BP neural
 296 network method to process the SST data with nonlinearity and non-stationarity. Through EEMD and CEEMD
 297 algorithms, SSTA time-series data are decomposed into different IMFs and a residue RES. BP neural network
 298 is applied to predict individual IMFs and the residue RES. Final results can be obtained by adding the

299 predicting results of individual IMFs and RES.

300 In order to illustrate the effectiveness of the proposed approach, a case study was carried out. SSTA
301 prediction results based on the hybrid EEMD-BPNN model and the hybrid CEEMD-BPNN model are
302 discussed. In comparison, the proposed hybrid CEEMD-BPNN model is much better and its prediction results
303 are more accurate.

304 From the absolute error of the prediction results of each component IMF and the absolute error of the
305 predicted SSTA, the prediction error of SSTA mainly comes from the prediction of the first three mode
306 decomposition components (IMF1, IMF2 and IMF3). SSTA prediction has been only preliminary, based on the
307 two improved EMD algorithms and BP neural network in this paper. The results show that the hybrid
308 CEEMD-BPNN model is more accurate in predicting SSTA. This work can provide a reference for predicting
309 SSTA and El Niño in the future. In the follow-up study, how to improve the forecast duration is the focus of
310 this work.

311 It should be noted that some factors affecting the SSTA prediction results include: the length and interval
312 of the time series of the database, as well as different data sources because their values are also different. The
313 SSTA time-series data in this study is based on NOAA Optimum Interpolation Sea Surface Temperature
314 (OISST) datasets from January 1982 to December 2016.

315

316 **Acknowledgement**

317 This work was supported by National Natural Science Foundation of China (Grant Nos. 51809023,
318 51879015, 51839002, 51809021 and 51509023).

319

320 **References:**

321 Amezquita-Sanchez, J. P. and Adeli, H.: A new music-empirical wavelet transform methodology for time–
322 frequency analysis of noisy nonlinear and non-stationary signals, *Digit. Signal Process.*, 45, 55-68,
323 <https://doi.org/10.1016/j.dsp.2015.06.013>, 2015.

324 Banzon, V., Smith, T. M., Chin, T. M., Liu, C., and Hankins, W.: A long-term record of blended satellite and
325 in situ sea-surface temperature for climate monitoring, modeling and environmental studies, *Earth Syst.*
326 *Sci. Data*, 8, 165-176, <https://doi.org/10.5194/essd-8-165-2016>, 2016.

327 Bond, N. A., Cronin, M. F., Freeland, H., and Mantua N.: Causes and impacts of the 2014 warm anomaly in
328 the NE Pacific. *Geophys. Res. Lett.*, 42, 3414-3420, <https://doi.org/10.1002/2015GL063306>, 2015.

329 Buckley, M. W., Ponte, R. M., Forget, G., and Heimbach, P.: Low-frequency SST and upper-ocean heat
330 content variability in the North Atlantic, *J. Climate*, 27, 4996-5018, [https://doi.org/10.1175/JCLI-D-13-](https://doi.org/10.1175/JCLI-D-13-00316.1)
331 00316.1, 2014.

332 Chen, C., Cane, M. A., Henderson, N., Lee, D. E., Chapman, D., Kondrashov D., and Chekroun, M. D.:
333 Diversity, nonlinearity, seasonality, and memory effect in ENSO simulation and prediction using
334 empirical model reduction, *J. Climate*, 29: 1809-1830, <https://doi.org/10.1175/JCLI-D-15-0372.1>,
335 2016b.

336 Chen, Z., Wen, Z., Wu, R., Lin X., and Wang J.: Relative importance of tropical SST anomalies in maintaining
337 the Western North Pacific anomalous anticyclone during El Niño to La Niña transition years, *Clim.*
338 *Dynam.*, 46, 1027-1041, <https://doi.org/10.1007/s00382-015-2630-1>, 2016a.

339 Cheng, Y., Ezer, T., Atkinson, L. P., and Xu, Q.: Analysis of tidal amplitude changes using the EMD method,
340 *Cont. Shelf Res.*, 148: 44-52, <https://doi.org/10.1016/j.csr.2017.09.009>, 2017.

341 Deo, M. C., Jha, A., Chaphekar, A. S., and Ravikant, K.: Neural networks for wave forecasting, *Ocean Eng.*,
342 28: 889-898, [https://doi.org/10.1016/S0029-8018\(00\)00027-5](https://doi.org/10.1016/S0029-8018(00)00027-5), 2001.

343 Duan, W. Y., Han, Y., Huang, L. M., Zhao, B. B., and Wang, M. H.: A hybrid EMD-SVR model for the short-
344 term prediction of significant wave height, *Ocean Eng.*, 124, 54-73,
345 <https://doi.org/10.1016/j.oceaneng.2016.05.049>, 2016.

346 Duan, W., Huang, L., Han Y., and Huang D.: A hybrid EMD-AR model for nonlinear and non-stationary
347 wave forecasting, *J Zhejiang Univ-Sc A*, 17(2): 115-129, <https://doi.org/10.1631/jzus.A1500164>, 2016.

348 Ezer, T. and Atkinson, L. P.: Accelerated flooding along the US East Coast: on the impact of sea - level rise,
349 tides, storms, the Gulf Stream, and the North Atlantic oscillations, *Earths Future*, 2, 362-382,
350 <https://doi.org/10.1002/2014EF000252>, 2014.

351 Griffies, S. M., Winton, M., Anderson, W. G., Benson, R., Delworth, T. L., Dufour, C. O., Dunne, J. P.,
352 Goddard, P., Morrison, A. K., Rosati, A., Wittenberg, A. T., Yin, J., and Zhang, R.: Impacts on ocean
353 heat from transient mesoscale eddies in a hierarchy of climate models. *J. Climate*, 28, 952-977,
354 <https://doi.org/10.1175/JCLI-D-14-00353.1>, 2015.

355 He, J., Deser, C., and Soden, B. J.: Atmospheric and oceanic origins of tropical precipitation variability. *J.*
356 *Climate*, 30, 3197-3217, <https://doi.org/10.1175/JCLI-D-16-0714.1>, 2017.

357 Huang, N. E., Shen, Z., Long, S. R., Wu, M. C., Shih, H. H., Zheng, Q., Yen, N., Tung, C. C., and Liu, H. H.:
358 The empirical mode decomposition and the Hilbert spectrum for nonlinear and non-stationary time

359 series analysis, *P. Roy. Soc. A-Math. Phys.*, 454, 903-995. <https://doi.org/10.1098/rspa.1998.0193>, 1998.

360 Huang, N. E. and Wu, Z.: A review on Hilbert - Huang transform: Method and its applications to geophysical
361 studies, *Rev. Geophys.*, 46, RG2006, <https://doi.org/10.1029/2007RG000228>, 2008.

362 Hudson, D., Alves, O., Hendon, H. H., Wang, G.: The impact of atmospheric initialisation on seasonal
363 prediction of tropical Pacific SST, *Clim. Dynam.*, 36, 1155-1171, [https://doi.org/10.1007/s00382-010-](https://doi.org/10.1007/s00382-010-0763-9)
364 0763-9, 2011.

365 Jain, P. and Deo, M. C.: Neural networks in ocean engineering, *Ships Offshore Struc.*, 1, 25-35,
366 <https://doi.org/10.1533/saos.2004.0005>, 2006.

367 Khan, M. Z. K., Sharma, A., and Mehrotra, R.: Global seasonal precipitation forecasts using improved sea
368 surface temperature predictions, *J Geophys. Res. -Atmos.*, 122, 4773-4785,
369 <https://doi.org/10.1002/2016JD025953>, 2017,

370 Kim, Y., Kim, H., and Ahn, I. G.: A study on the fatigue damage model for Gaussian wideband process of
371 two peaks by an artificial neural network, *Ocean Eng.*, 111, 310-322,
372 <https://doi.org/10.1016/j.oceaneng.2015.11.008>, 2016.

373 Kumar, M., Parmar, C., Chaudhary, V., Kumar, A., and SST-1 team.: Observation of plasma shift in SST-1
374 using optical imaging diagnostics, *J Phys. Conf. Ser.*, 823, 012056, [https://doi.org/10.1088/1742-](https://doi.org/10.1088/1742-6596/823/1/012056)
375 6596/823/1/012056, 2017.

376 Lee, H. S.: Estimation of extreme sea levels along the Bangladesh coast due to storm surge and sea level rise
377 using EEMD and EVA, *J Geophys. Res.-Oceans*, 118, 4273-4285, <https://doi.org/10.1002/jgrc.20310>,
378 2013,

379 Lee, T. L.: Back-propagation neural network for long-term tidal predictions, *Ocean Eng.*, 31, 225-238,
380 [https://doi.org/10.1016/S0029-8018\(03\)00115-X](https://doi.org/10.1016/S0029-8018(03)00115-X), 2004.

381 López, I., Aragonés, L., Villacampa, Y., and Serra, J. C.: Neural network for determining the characteristic
382 points of the bars, *Ocean Eng.*, 136: 141-151, <https://doi.org/10.1016/j.oceaneng.2017.03.033>, 2017.

383 Monteiro, E., Yvonnet, J., He, Q. C.: Computational homogenization for nonlinear conduction in
384 heterogeneous materials using model reduction. *Comp. Mater. Sci.*, 42, 704-712,
385 <https://doi.org/10.1016/j.commatsci.2007.11.001>, 2008.

386 Motulsky, H. J. and Ransnas, L. A.: Fitting curves to data using nonlinear regression: a practical and
387 nonmathematical review, *Faseb J.*, 1, 365-374. <https://doi.org/10.1096/fasebj.1.5.3315805>, 1987.

388 Pan, H., Guo, Z., Wang, Y., and Lv, X.: Application of the EMD method to river tides, *J. Atmos. Ocean. Tech.*,

389 35, 809-819, <https://doi.org/10.1175/JTECH-D-17-0185.1>, 2018.

390 Pearson, R. K. and Pottmann, M.: Gray-box identification of block-oriented nonlinear models, *J. Process*
391 *Contr.*, 10, 301-315, [https://doi.org/10.1016/S0959-1524\(99\)00055-4](https://doi.org/10.1016/S0959-1524(99)00055-4), 2000.

392 Reynolds, R. W., Smith, T. M., Liu, C., Chelton, D. B., Casey, K. S., and Schlax., M. G.: Daily high-
393 resolution-blended analyses for sea surface temperature, *J. Climate*, 20, 5473-5496,
394 <https://doi.org/10.1175/2007JCLI1824.1>, 2007.

395 Sadeghifar, T., Motlagh, M. N., Azad, M. T., and Mahdizadeh, M. M.: Coastal wave height prediction using
396 Recurrent Neural Networks (RNNs) in the south Caspian Sea, *Mar. Geod.*, 40, 454-465,
397 <https://doi.org/10.1080/01490419.2017.1359220>, 2017.

398 Savitha, R. and Mamun, A. A.: Regional ocean wave height prediction using sequential learning neural
399 networks, *Ocean Eng.*, 129: 605-612, <https://doi.org/10.1016/j.oceaneng.2016.10.033>, 2017.

400 Sukresno, B., Hanintyo, R., Kusuma, D. W., Jatisworo, D., and Murdimanto., A.: Three-way error analysis
401 of sea surface temperature (SST) between HIMAWARI-8, buoy, and mur SST in SAVU Sea, *Int. J.*
402 *Remote Sens. Earth Sci.*, 15, 25-36, <https://doi.org/10.30536/j.ijreses.2018.v15.a2855>, 2018,

403 Takakura, T., Kawamura, R., Kawano, T., Ichiyangi, K., Tanoue, M., and Yoshimura, K.: An estimation of
404 water origins in the vicinity of a tropical cyclone's center and associated dynamic processes, *Clim.*
405 *Dynam.*, 50, 555-569, <https://doi.org/10.1007/s00382-017-3626-9>, 2018.

406 Tang, L., Dai, W., Yu, L., and Wang, S.: A novel CEEMD-based EELM ensemble learning paradigm for crude
407 oil price forecasting, *Int. J. Inf. Tech. Decis.*, 14, 141-169, <https://doi.org/10.1142/S0219622015400015>,
408 2015.

409 Wang, S., Zhang, N., Wu, L., and Wang, Y.: Wind speed forecasting based on the hybrid ensemble empirical
410 mode decomposition and GA-BP neural network method, *Renew. Energ.*, 94, 629-636,
411 <https://doi.org/10.1016/j.renene.2016.03.103>, 2016.

412 Wang, W., Chau, K., Xu, D., and Chen, X.: Improving forecasting accuracy of annual runoff time series using
413 ARIMA based on EEMD decomposition, *Water Resour. Manag.*, 29, 2655-2675,
414 <https://doi.org/10.1007/s11269-015-0962-6>, 2015.

415 Wang, W., Tang, R., Li, C., Liu, P., and Luo, L.: A BP neural network model optimized by Mind Evolutionary
416 Algorithm for predicting the ocean wave heights, *Ocean Eng.*, 162, 98-107,
417 <https://doi.org/10.1016/j.oceaneng.2018.04.039>, 2018.

418 Wang, Y., Wilson, P. A., Zhang, M., and Liu, X.: Adaptive neural network-based backstepping fault tolerant

419 control for underwater vehicles with thruster fault, *Ocean Eng.*, 110, 15-24,
420 <https://doi.org/10.1016/j.oceaneng.2015.09.035>, 2015.

421 Wiedermann, M., Donges, J. F., Handorf, D., Kurths, J., and Donner, R. V.: Hierarchical structures in
422 Northern Hemispheric extratropical winter ocean–atmosphere interactions, *Int. J. Climatol.*, 37, 3821-
423 3836, <https://doi.org/10.1002/joc.4956>, 2017.

424 Wu, L. C., Kao, C. C., Hsu, T. W., Jao K. C. and Wang, Y. F.: Ensemble empirical mode decomposition on
425 storm surge separation from sea level data, *Coast. Eng. J.*, 53, 223-243,
426 <https://doi.org/10.1142/S0578563411002343>, 2011.

427 Wu Z., Schneider E. K. and Kirtman B. P.: The modulated annual cycle: an alternative reference frame for
428 climate anomalies, *Clim. Dyna.*, 31(7-8): 823-841, <https://doi.org/10.1007/s00382-008-0437-z>, 2008.

429 Wu, Z. and Huang, N. E.: Ensemble empirical mode decomposition: a noise-assisted data analysis method,
430 *Adv. Adap. Data Anal.*, 1, 1-41, <https://doi.org/10.1142/S1793536909000047>, 2009.

431 Wu Z., Jiang C., Chen J., Long Y., Deng B. and Liu X.: Three-Dimensional Temperature Field Change in the
432 South China Sea during Typhoon Kai-Tak (1213) Based on a Fully Coupled Atmosphere–Wave–Ocean
433 Model, *Water*, 11(1): 140, <https://doi.org/10.3390/w11010140>, 2019a.

434 Wu Z., Jiang C., Deng B., Chen J., Long Y., Qu K. and Liu X.: Numerical investigation of Typhoon Kai-tak
435 (1213) using a mesoscale coupled WRF-ROMS model, *Ocean Eng.*, 175: 1-15.
436 <https://doi.org/10.1016/j.oceaneng.2019.01.053>, 2019b.

437 Yeh, J. R., Shieh, J. S., and Huang, N. E.: Complementary ensemble empirical mode decomposition: A novel
438 noise enhanced data analysis method, *Adv. Adap. Data Anal.*, 2, 135-156,
439 <https://doi.org/10.1142/S1793536910000422>, 2010.

440 Zheng, X. T., Xie, S. P., Lv, L. H., and Zhou, Z. Q.: Intermodel uncertainty in ENSO amplitude change tied
441 to Pacific Ocean warming pattern, *J. Climate*, 29, 7265-7279, <https://doi.org/10.1175/JCLI-D-16-0039.1>,
442 2016.

443 Zhu, J., Huang, B., Kumar, A., and Kinter, J. L.: Seasonality in prediction skill and predictable pattern of
444 tropical Indian Ocean SST, *J. Climate*, 28, 7962-7984, <https://doi.org/10.1175/JCLI-D-15-0067.1>, 2015.